PROCEEDINGS, 43rd Workshop on Geothermal Reservoir Engineering
Stanford University, Stanford, California, February 12-14, 2018
SGP-TR-213

Experimental Study on Injection-induced Fracture Propagation and Coalescence for EGS Stimulation

Zhi Ye and Ahmad Ghassemi

Reservoir Geomechanics and Seismicity Research Group, The University of Oklahoma, Norman, OK 73019

ahmad.ghassemi@ou.edu

Keywords: fracture coalescence, mixed-mode fracture, permeability enhancement, injection experiment, EGS stimulation, wing cracks

ABSTRACT

Shear slip has been recognized as a dominant mechanism of permeability enhancement during the hydraulic stimulation in engineered geothermal systems (EGS). The so-called "hydroshearing" process usually occurs at treatment pressures below the minimum principal stress, and reactivates pre-existing fractures causing them to slip and dilate and possibly propagate in the shear and tensile modes creating new cracks. These processes can result in generation of a network with increased permeability for economic flow rates. We have performed injection experiments to investigate the possibility of flow rate increase through the propagation and coalescence of pre-existing fractures in granites under triaxial conditions. Results show that the pre-existing fractures can be propagated and coalesce at treatment pressures lower than the minimum principal stress during water injection. Also significant flow rate increase can be achieved through the fracture network generation caused by pre-existing fractures propagation and coalescence. In addition, both tensile wing cracks, shear and/or mixed-mode propagated secondary cracks can form. These observations show that the so called "hydroshearing" involves both shear slip and fracture propagation and contribute to the shear stimulation in EGS.

1. INTRODUCTION

Significant high grade geothermal resources occur in low permeability rocks which would require permeability enhancement, which has led to the concept of Enhanced Geothermal Systems (EGS). The shear simulation concept has been considered as the main approach to permeability creation by reactivating natural fractures to slip and prop-open by water injection (Pine and Batchelor 1984, Willis-Richards, et al. 1996, Baria, et al. 1999, Rahman, et al. 2002, Nygren and Ghassemi 2005, Cheng and Ghassemi 2016). Permeability increase due to shear slip has been demonstrated in laboratory scale direct shear-flow tests (Esaki, et al. 1991, Yeo, et al. 1998, Li, et al. 2008, Park, et al. 2013) and triaxial shear-flow tests on samples with manually displaced fractures (Durham and Bonner 1994, Zhang, et al. 2013, Crawford, et al. 2016, Hofmann, et al. 2016) or samples with saw-cut fractures (Nemoto, et al. 2008, Bauer, et al. 2016). Also, the injection-induced shear slip tests on rough granite fractures under triaxial condition have been performed and the results clearly show significant enhanced flow rates can be achieved during the shearing of fractures (Ye, et al. 2017a, 2017b, 2017c). This is to be expected because under appropriate reservoir conditions, secondary cracks can be an integral part of shear slip stimulation mechanism as shear slip increases the stress-intensity at the fracture tips, potentially leading to fracture propagation. These processes have been implicitly and/or explicitly considered in Soultz EGS (Evans, et al. 2005, Evans 2005, Cornet, et al. 2007, Jung 2013) and have led to efforts for mixed-mode fracture propagation model development for EGS (Min, et al. 2010, Huang, et al. 2013). The formation of wing-cracks is particularly the case when the natural fractures are directly subjected to water injection as shown in numerical models (Min, et al. 2010, Jung 2013, McClure and Horne 2013, Kamali and Ghassemi 2016). However, there are few experimental data to verify the production increase resulting from injection-induced fracture slip and propagation during shear stimulation. Most experimental studies that have considered the cracking behavior of pre-existing fracture propagation have used artificial materials (glass, ice, Columbia resin, concrete, PMMA, etc.) rather than real rocks (Brace and Bombolakis 1963, Nemat-Nasser and Horii 1982, Ashby and Hallam 1986, Cannon, et al. 1990) and have been mainly limited to uniaxial (Miller and Einstein 2008, Wong and Einstein 2009, Yin, et al. 2010, Lee and Jeon 2011, Modiriasari et al. 2016) or biaxial compression (Petit and Barquins 1988, Bobet and Einstein 1998, Saimoto and Nisitani 2002, Mughieda and Karasneh 2006, Liu, et al. 2016). A few researchers have conducted triaxial tests (Yang, et al. 2008, Huang, et al. 2016) or injection tests under biaxial compression (Goncalves da Silva, et al. 2015, Morgan, et al. 2017) on pre-existing fractures. Results of these tests have been used to investigate cracking modes of the fractures, or the process of fracture propagation and coalescence, or failure behavior and deformation properties without addressing flow. In addition, the few injection tests on pre-existing fractures have been conducted under biaxial compression condition with extremely low injection pressure (~ 5MPa) due to sealing issues. To our knowledge, no experiments have been completed that directly induce fracture propagation and coalescence under triaxial loading through high pressure injection. The effects of water injection pressure applied inside the fractures and confining pressure on fractures cracking behavior are not well understood. Moreover, the production evolution with the fracture propagation, coalescence and fracture network generation, which highly related to the subsurface energy extraction, has not been fundamentally explored through the laboratory scale tests.

In this pioneering study, injection-induced fracture propagation tests were performed on the single-flawed and double-flawed granite samples, receptivity. The observations in the single-flawed sample SW-1 is used to prove that the pre-existing fractures can be propagated at the treatment pressure below minimum principal stress during injection. Whereas the tests of double-flawed sample SW-2 shows that the fractures are able to be propagated and coalesced to generate fracture networks during shearing stimulation, and the significant flow rate increase was achieved through the fracture propagation and coalescence. All these observations and experimental results would help understanding the cracking behavior and fluid flow in shear stimulation of EGS.

2. EXPERIEMENT METHODS

2.1 Sample materials and preparation

The samples used in this study are cylindrical Sierra White granite cores with 50.8 mm (2-inch) diameter by 101.6 mm (4-inch) length. Some important mechanical properties, such as Young's modulus, Poisson's ratio, Uniaxial Compressive Strength, tensile strength, etc., were determined by a series of regular uniaxial/triaxial test and Brazilian tests. In addition, the matrix permeability of this granite was measured as 500-1000 Nano-Darcy through the permeability tests on 25 mm diameter granite discs with 12.5 mm thickness. The results of these properties are shown in Table 1. The powder X-ray diffraction analysis shown that quartz and albite dominate the mineral contents of this Sierra White granite.

Table 1: Mechanical properties and matrix permeability of the Sierra White granite

Young's Modulus, GPa	Poisson's Ratio	UCS, MPa	Tensile Strength, MPa	Friction Angle	Cohesion, MPa	Matrix Permeability, Nano-Darcy
67	0.32	150	11	46°	30	500-1000

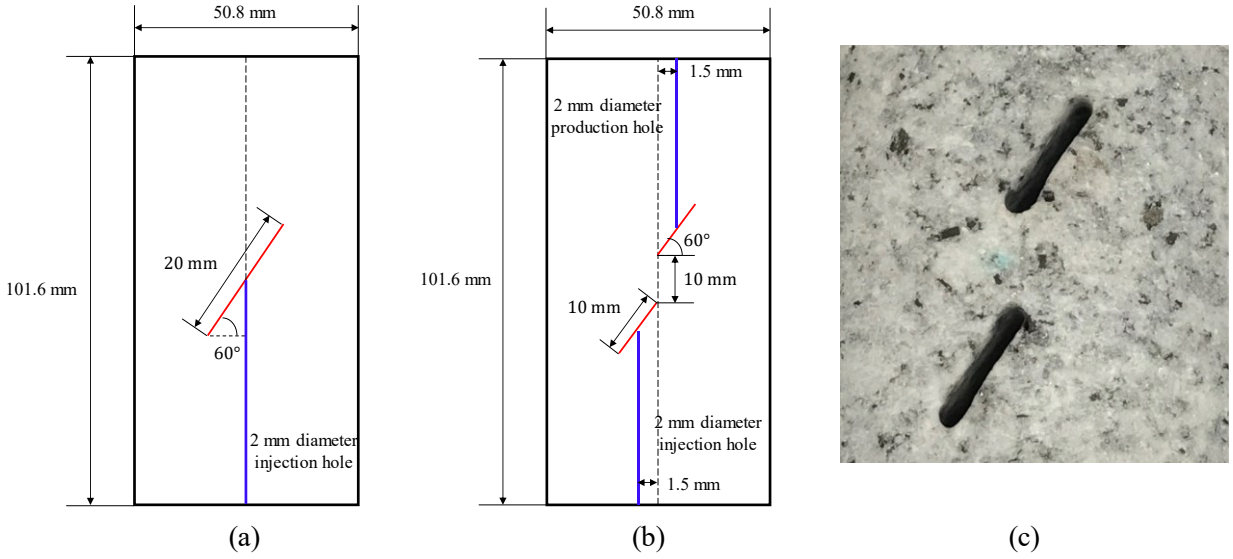

Figure 1: (a) sketch of single-flawed sample; (b) sketch of double-flawed sample; (c) waterjet cut fractures with "keyhole" tip.

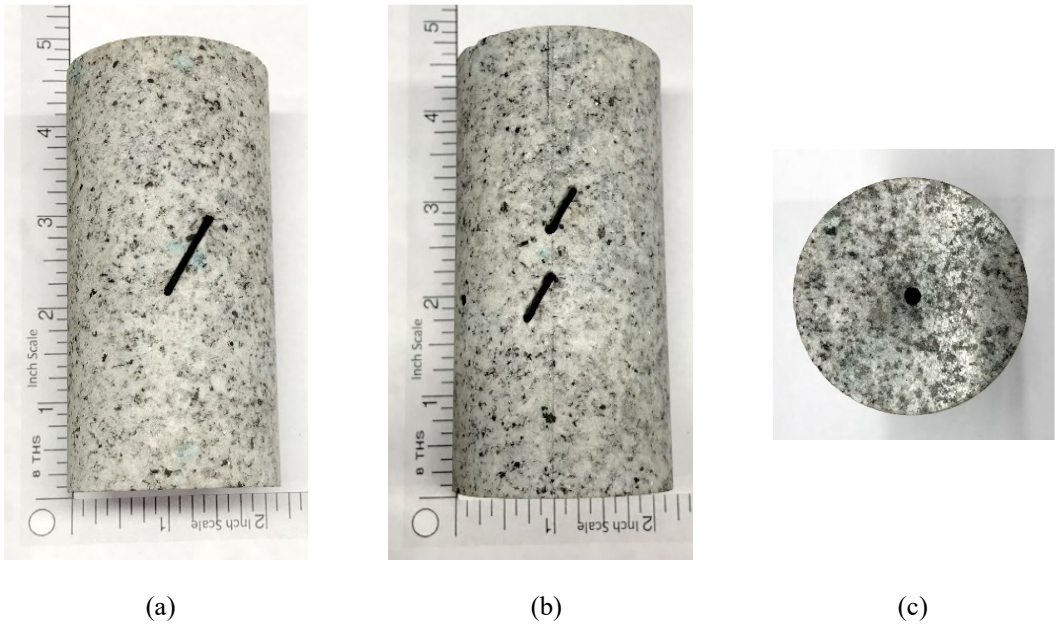

Figure 2: (a) single-flawed sample SW-1; (b) double-flawed sample SW-2; (c) injection hole on the surface end.

To create the cylindrical granite samples with a single or double pre-cut fractures, a commercial water-jet system was used to create flaws in the granite samples. Pressurized water mixed with a garnet abrasive sands ejected from a 1 mm diameter nozzle created the flaws with an average 1.6 mm width. As shown in Figure 1(a), the single-flawed sample (sample SW-1) located in the center of the sample contains a 20 mm length inclined fracture, and the inclination angle from fracture to the short axis of the sample is 60º. In the case to double-flawed sample (sample SW-2, see Figure 1(b)), two fractures located each side of the central axis of the sample both have an inclination angle of 60º, while they are only 10 mm long. The bridge length of the two parallel fractures is also 10 mm. In the Figure 1(c), it is observed that the waterjet cut flaw has a round tip (the so called "keyhole") which is a little wider at the starting point because of the waterjet first creates a hole to penetrate the sample. In addition, injection holes (2 mm diameter) were drilled into the flaws to form fluid flow paths. For single-flawed sample, one injection hole was drilled along central axis of the sample from the bottom end to fracture surface; for the double-flawed sample, two holes (1.5 mm far from the central axis of the sample) were drilled from the two sample ends to touch the top flaw and the bottom flaw, respectively. The injection hole only touches one surface of the fracture and does not cross it. The samples with pre-cut fractures and injection hole are shown in Figure 2.

2.2 Experiment setup and measurements

The injection fracturing tests were carried out using an MTS 816 frame, which has a maximum 1000 kN axial load and includes a triaxial cell with 138 MPa (20,000 psi) confining pressure capacity. Control and data acquisition were performed using MTS Series 793TM Control software. The setup of the tests with pre-cut flaws are sketched in Figure 3. During the injection tests, the average axial displacement of the rock sample is measured by two Linear Variable Differential Transformer (LVDT) position sensors. Another LVDT attached on a radial ring is used to record transverse displacement. The associated error of this type AC-LVDT is ±0.05%. Whereas the force is measured by a load-cell located inside of the triaxial pressure vessel with maximum 1 KN loading error. Teledyne ISCO 100DM syringe pumps (68.95 MPa pressure limit, 25 ml/min flowrate limit and 103 mL volume capacity) are used to inject/produce water and measure related the flow parameters (pressure, flow rate and pump volume). The ISCO pump has a ±0.5 % pressure error and ±0.3 % flow rate error, resulting in maximum errors of 0.35 MPa pressure and 0.075 ml/min flow rate, respectively. As shown in Figure 3(a), water is injected into the fracture from the bottom hole of the single-flawed sample by a syringe pump to induce fracture propagation. For the double-flawed sample in Figure 3(b), water is injected into the lower fracture from the bottom hole by pump A to induce fracture propagation. The production pressure in pump B is kept as constant with a low value. Therefore, once the lower fracture coalesces with the upper fracture, water is produced from the top hole to pump B due to the pressure difference of the two pumps.

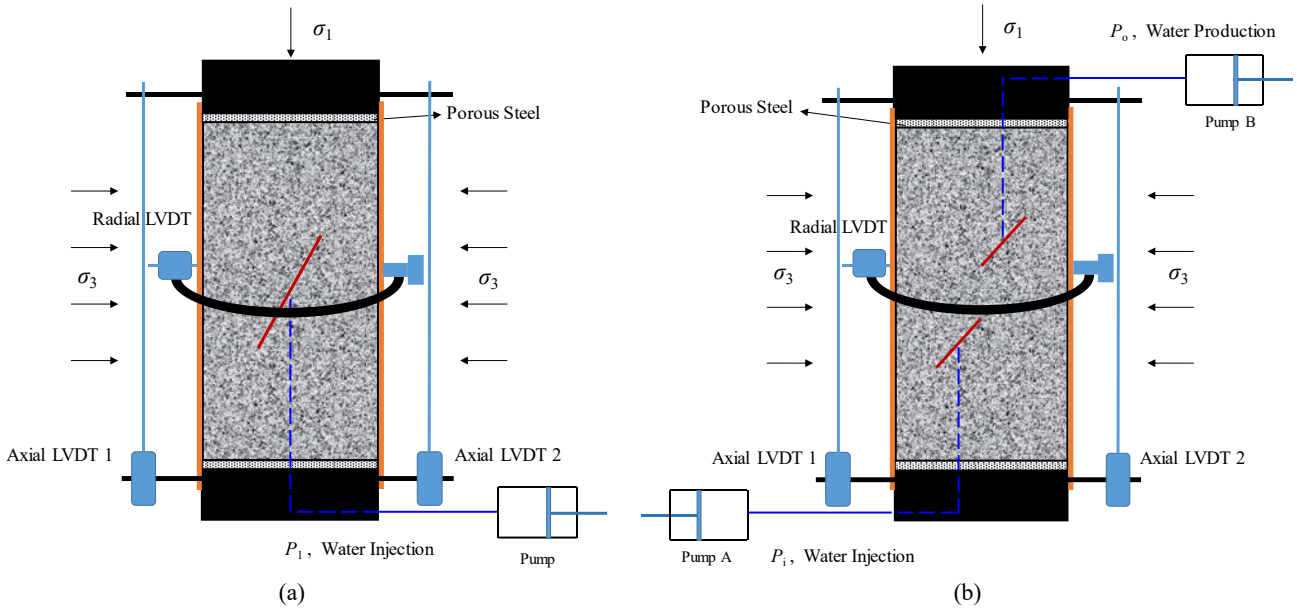

Figure 3: Sketch of sample setup and fluid flow: (a) single-flawed sample; (b) double-flawed sample.

3. EXPERIEMENT RESULTS

In this study, we focus on two main issues: one is injection-induced fracture propagation in a single-flawed sample (SW-1); the other issue is fracture propagation and coalescence in a double-flawed sample (SW-2) during water injection, as well as the flow rate enhancement upon fracture network generation in response to injection-induced fracture propagation and coalescence. These are discussed below based on experimental observations.

3.1 Test 1 – Single-flawed sample

To characterize the cracking behavior of pre-existing or natural fractures, an injection fracturing test was conducted on the single-flawed sample SW-1 where fracture propagation was induced by injection pressures below the confining pressure. As shown in Figure 3(a), during the test, a 30 MPa confining pressure is firstly applied on the sample. After that, the sample is loaded to a reference value of differential stress and then the test is switched to a constant displacement control mode which keeps the loading piston displacement of

the MTS 816 frame constant during the injection process. Next, the injection pressure is gradually increased at a constant rate (0.15 MPa/sec.) from 0 MPa to 29 MPa to induce fracture propagation. During the test, mechanical properties (axial displacement, radial displacement, and differential stress) and flow parameters (flow rate, pressure and pump volume) are all measured to characterize the hydro-mechanical response of the fracture in the propagation process.

The test results during injection are shown in Figure 4, the deformation properties and flow parameters during confining pressure increase and axial loading on the sample in the pre-injection stage are not shown in this graph which means the displacements and flow rates are zeros before injection. In Figure 4, the green curve represents the loading piston displacement of the MTS 816 frame, kept as constant under a constant displacement control mode during the injection process; the differential stress is plotted using the black curve, which significantly drops as the fracture propagates (because the compression exerted on the sample decreases with gradual propagation of the fracture); the blue curve shows the injection pressure and consists of a pressure buildup stage when the injection pressure is continuously increased at constant rate, and a pressure hold stage when the pressure is kept as constant; the axial displacement and radial displacement are illustrated by the red and pink curves, respectively; the purple curve shows the flow rate caused by injection by the syringe pump; the cyan curve shows the volume of injection pump. To characterize the crack types after testing, the sample SW-1 was cut axially in two halves. A fluorescer was used to detect the morphology of the fractures under ultraviolet light. The sample surface (side wall) and the surface of the central cut, as well as the corresponding fluoresced pictures are shown in Figure 5. In Figure 5(a1) and Figure 5(b1), the black arrows indicate the injection direction (water was injected from bottom to up).

The wing cracks or primary cracks are usually found to be the first fractures emanating from the pre-existing flaws, and always initiated from the tips of the pre-existing flaws. Often, wing cracks induced by tensile stress are thin without branches. A pair of wing cracks can be found on the side wall of the specimen in Figure 5(a2) and on the central surface shown in Figure 5(b2); they are both a thin single crack without any branches. On the other hand, two secondary cracks, which are wider and longer than the wing cracks are also detected on the tested sample SW-1. Unlike the wing cracks, the secondary cracks initiated at a distance away from the flaw tips. Moreover, the secondary cracks appear to be of mixed mode type which initially opened as tensile cracks and then propagated in shear. The shear zones with multiple crack branches on the tails of the secondary cracks are clear indications of this mixed-mode crack propagation. The shape and length of major cracks on the sidewall and on the central cut section are similar, however, the branches in shear zones propagating from the tails of the secondary cracks are not identical.

Considering the morphology of the propagated cracks, the water injection process in Figure 4 can be divided into five zones. Zone I is the crack nucleation zone (light-gray zone), where micro-cracks were nucleated due to the stress field caused by increased injection pressure. The first jump in the measurements of deformation properties and flow parameters is observed in Zone II (light-golden zone), the increased displacements (axial and radial) and the decreased differential stress represent propagation of cracks formed in Zone I, resulting in rapid flow rate increase. After that, a stable fracture propagation zone (Zone III, light-blue zone) is noticed on the graph with gradual changes in displacements, stress, and pump volume until the second jump zone. In the second jump zone (Zone IV, light-golden color), much larger changes of stress drop, displacements increase, and flow rate increase can be observed. Considering the wider and longer secondary cracks in Figure 5, it is reasonable to assume the second jump is caused by the fast propagation of secondary cracks since they initiated later than the wing cracks. The last zone is a stable propagation zone (Zone V, light-blue color), it can be inferred that secondary cracks continually propagated to form shear branches at their tails, while the propagation of primary wing cracks was restricted due to the secondary cracks taking more fluid. The secondary cracks can be longer than the primary wing cracks, a feature that is similar to some previous experimental fracture propagation tests under uniaxial compression (Chen, et al. 1992, Wong and Einstein 2009, Lee and Jeon 2011).

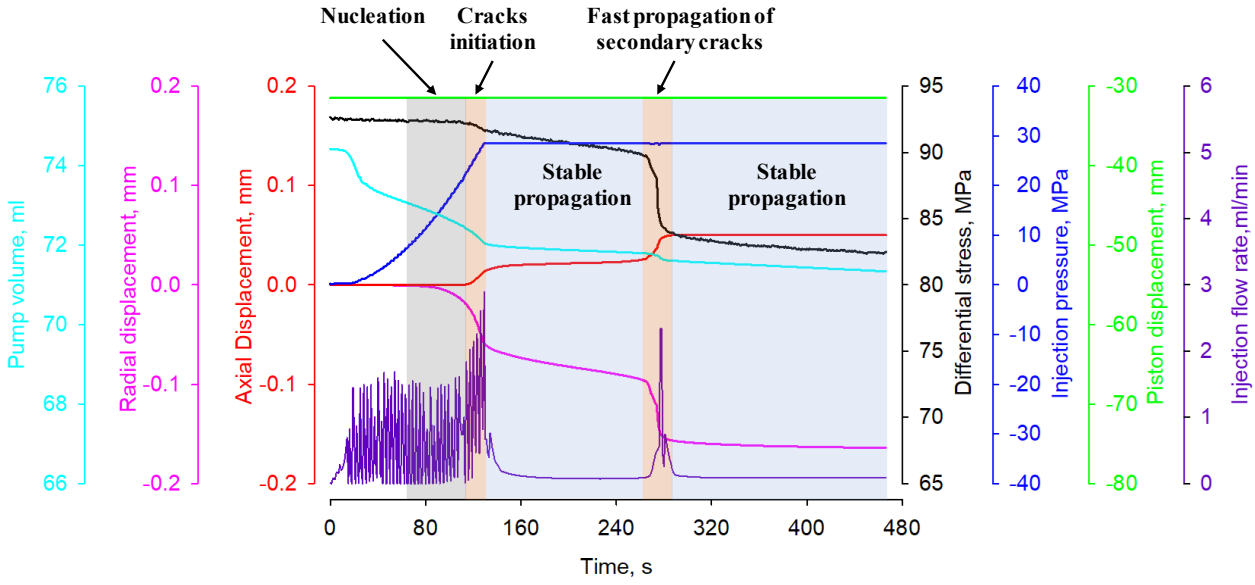

Figure 4: Injection-induced fracture propagation test on single-flawed sample SW-1.

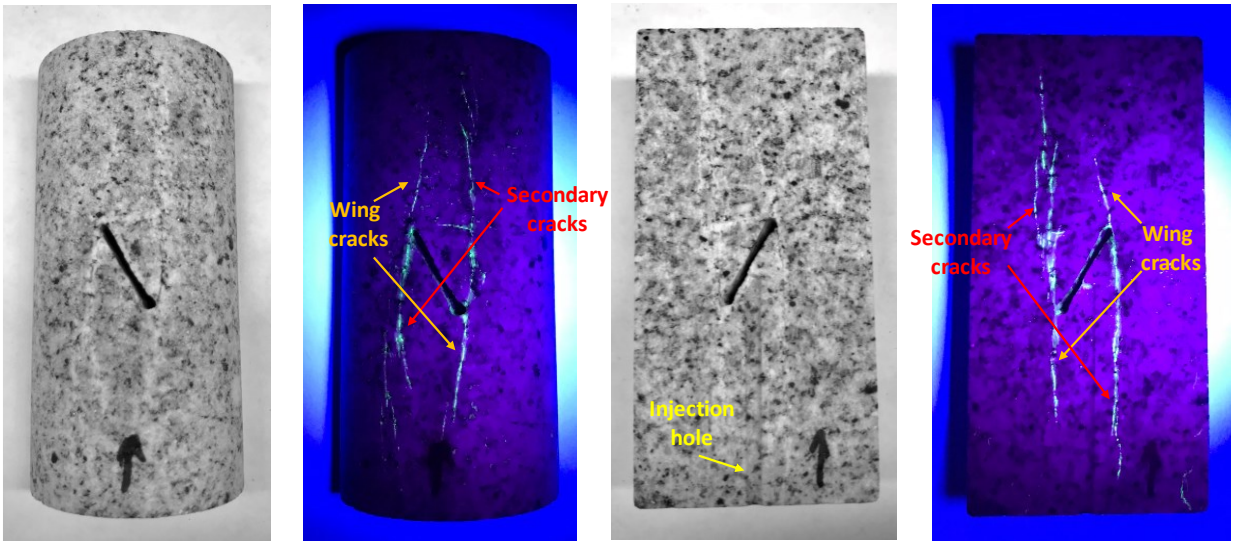

(a1) (a2) (b1) (b2)

Figure 5: The morphology of cracks on tested sample SW-1: (a1) the side wall; (a2) fluoresced cracks at the side wall; (b1) the surface of the central cut; (b2) fluoresced cracks at the surface of the central cut.

3.2 Test 2 – Double-flawed sample

The purpose of Test 1 was to illustrate that fractures can be propagated even at treatment pressures below the minimum principal stress. In Test 2, injection was conducted on the double-flawed sample to investigate the fracture network generation resulting from pre-existing or natural fractures propagation and coalescence, and to verify the possibility of flow rate increase during the process of fracture network generation. As shown in the Figure 3(b), in the Test 2, we firstly applied a 30 MPa confining pressure on the sample. The production pressure of pump B was set to a constant value of 5 MPa, while the injection pressure of pump A was set to an initial value of 5 MPa and later was raised to induce fracture propagation and coalescence. Then, the sample was loaded to a reference differential stress level and system control was switched to the constant displacement control mode. Next, the injection pressure was increased to 10 MPa and was held as constant for a period of 200 seconds to check whether the fracture would propagate at the low level of injection pressure. At last, the injection pressure was continually raised to 29 MPa to induce fracture propagation and coalescence. Likewise, the mechanical properties and flow parameters were also recorded during the whole test. Figure 6 is the test results on the sample SW-2 using the same color scheme as in the previous test except that the dark-yellow curve and dark-green curve reflect the production pressure and flow rate of pump B, respectively. After the test, the sample SW-2 was also cut in two halves along the central vertical axis to exhibit the crack types and coalescence emanating from the two pre-existing flaws. One half of the sample and the corresponding pictures of fluoresced cracks under ultraviolet light are shown in Figure 7. The black arrows in Figure 7(a1) and Figure 7(b1) show the direction of water flow (water was injected from the bottom hole and produced from the top hole).

As shown in Figure 7 (a2), it is noticed that two wing cracks emanated from the right tip of the upper flaw and the left tip of the lower flaw, and the wing crack of the lower flaw is longer than that of the upper flaw. Meanwhile, two secondary cracks also have formed at the same tips of the flaws (generally in direction opposite the wing crack). In addition, a tensile crack can be observed in the bridge area between the two pre-existing flaws. Here, the two wing cracks are longer than the secondary cracks and the bridge crack, but the secondary cracks contain multiple strands or branches (forming a shear zones) partially connected with the bridge crack to yield a fracture network. The secondary crack emanating from the lower tip of the lower flaw propagates upward and attempts to coalesce with the lower tip of the upper flaw. Whereas the secondary crack growing from the upper tip of the upper flaw, propagates downward and through its “horsetail” zone partially coalesces with the upper tip of the lower flaw and the bridge crack. Moreover, it can be seen that the long wing cracks separately propagated and crossed the wellbores (injection and production holes).

In the Figure 6, the process of injection-induced fracture propagation and coalescence on sample SW-2 can be divided into three zones with reference to the cracking behavior. Zone I marked with light-gray color is the cracks nucleation zone. In this zone, the sample’s radial expansion (expansion is negative using rock mechanics sign convention) gradually increased, while the axial deformation and differential stress changed slightly. This feature in the deformation record indicates that micro-cracks were opened and nucleated around the tips of pre-existing flaws but did not propagate since there were not sufficient axial deformation and differential stress drops. In the Zone II (light-golden color), both displacements (axial and radial) and differential stress display significant changes along with increase of the injection pressure, which means the cracks propagation was initiated. However, the lower flaw and the upper flaw did not coalesce with each other in Zone II since the flow rate of pump B was still zero. The last Zone III shown as light-blue color is the fracture coalescence zone where the flow rate of the pump B (dark green curve in Figure 6) shows continuous increase, and much larger deformations and stress drops are observed. In this zone, the two pre-existing flaws have completely coalesced through the bridge crack. Therefore, the water could flow from the lower flaw to the upper flaw. At the end of Zone III, the pump B almost has the same flow rate as which of

pump A indicating that all water injected by pump A was produced by pump B. Because the bridge crack dominated the flow once the two pre-existing flaws connected with each other, the propagation of secondary cracks was restricted (see Figure 7(a2) and Figure 7(b2)).

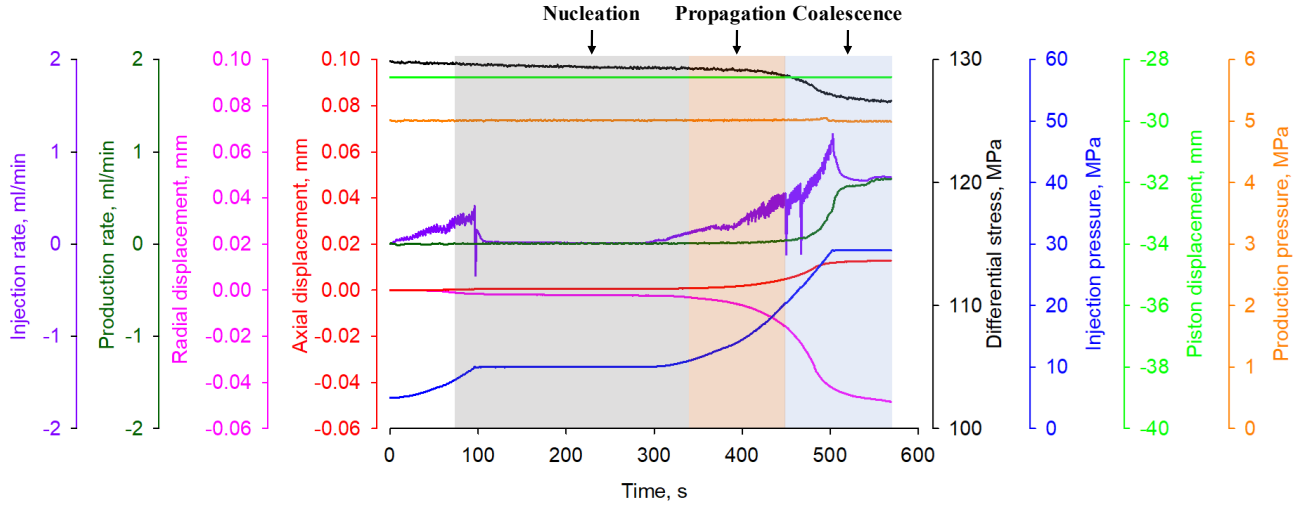

Figure 6: Injection-induced fracture propagation and coalescence test on double-flawed sample SW-2.

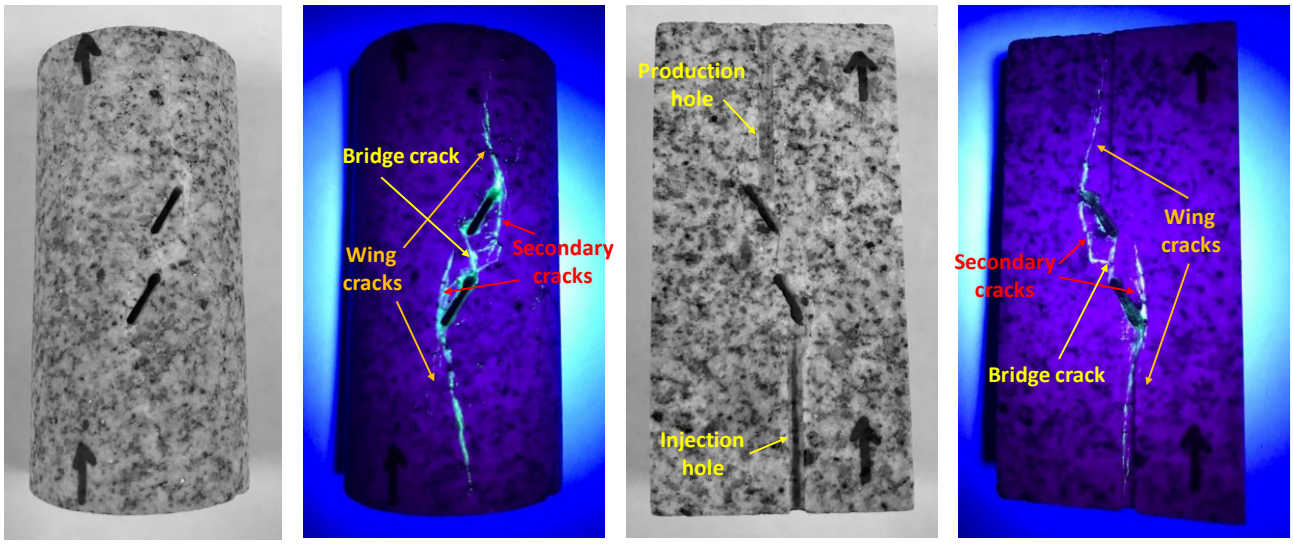

(a1) (a2) (b1) (b2)

Figure 7: The morphology of cracks on tested sample SW-2: (a1) the side wall; (a2) fluoresced cracks at the side wall; (b1) the surface of the central cut; (b2) fluoresced cracks at the surface of the central cut.

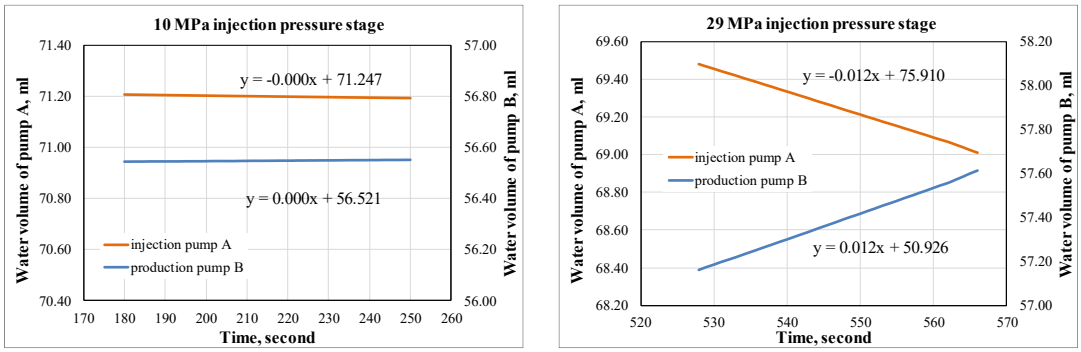

(a) (b)

Figure 8: The steady-state flow rates of pump A and pump B under two constant pressure hold stages: (a) 10 MPa injection pressure stage; (b) 29 injection pressure stage.

Another important issue in Test 2 is the possibility of production increase due to the fracture network generation caused by fracture propagation and coalescence. Two hold stages with constant injection pressures (10 MPa and 29 MP, respectively) were designed to compare the steady-state flow rates before and after fracture network generation. Figure 8(a) and Figure 8 (b) are used to illustrate the steady-state flow rates (Ye, et al. 2017) of the two pumps under 10 MPa injection pressure and 29 MPa injection pressure, respectively. In each plot of Figure 8, the x-axis is time while the two y-axes are separately the water volume of the injection pump A and the production pump B. Therefore, the slops of the curves are injection flow rate (orange curve) and production flow rate (blue curve), respectively. The negative flow rate of pump A represents injection due to its volume decreased during water injection, while the positive flow rate of pump B means production because of the water volume of pump B raised significantly after the pre-existing fractures coalescence. During the stage with constant 10 MPa injection pressure, both injection flow rate and production flow rate are almost zero, which means there was no fracture coalescence. Moreover, the zero flow rates also indicate that the cracks nucleation and fracture propagation are resulted from the change of stress field due to injection but not are directly originated from the fluid flow. On the other hand, at the later stage with constant 29 MPa injection pressure after fracture coalescence, both the injection flow rate and the production flow rate achieved remarkable increase and they were almost identical as 0.012 ml/min (all injection water from pump A was produced by pump B). Here, it is noticed that the steady-state flow rate is smaller than the corresponding transient flow rate.

4. CONCLUSION

In this research, we performed laboratory-scale injection tests on a single-flawed sample and a double-flawed sample (both are Sierra White granite), respectively. In the first test of the single-flawed sample SW-1, we verified that fractures do propagated at treatment pressures lower than minimum principal stress during water injection. Also, both tensile crack propagation and mixed-mode crack propagation were observed on the tested sample. In the test of the double-flawed sample SW-2, the pre-existing flaws successfully propagated and coalesced to generate a fracture network during water injection, resulting in a significant production increase and eventually all water injected was extracted from the production hole/well. In addition, corresponding changes in deformation properties (axial and radial displacements, stress) and flow parameters (flow rate, pump volume) have been definitely observed during the injection-induced fracture propagation and coalescence. Moreover, the crack formation modes correlate with the measurements of deformation properties and flow parameters, explaining the process of fracture propagation. Generally, there are four steps during the propagation and coalescence of fractures emanating from the pre-existing flaws in response to water injection: micro-cracks nucleation, onset of fractures propagation, stable propagation of fractures, and fractures coalescences. These observations resulting from this work, combined with our previous injection-induced shear slip tests, clearly indicate for the first time that both shear slip and fracture propagation (in tension and shear modes) are two fundamental and integral mechanisms for production increase during shear stimulation.

REFERENCES

Ashby, M. F., and Hallam, S. D.: The Failure of Brittle Solids Containing Small Cracks Under Compressive Stress States, *Acta Metallurgica*, **34**(3), (1986), 497-510.

Baria, R., et al.: HDR/HWR Reservoirs: Concepts, Understanding and Creation, *Geothermics*, **28**(4–5): (1999), 533-552.

Bauer, S. J., et al.: Experimental and Numerical Investigation of Hydro-Thermally Induced Shear Stimulation, *Proceedings*, 50th US Rock Mechanics/Geomechanics Symposium, American Rock Mechanics Association, Houston, TX (2016).

Bobet, A., and Einstein, H. H.: Fracture Coalescence in Rock-Type Materials Under Uniaxial and Biaxial Compression, *International Journal of Rock Mechanics and Mining Sciences*, **35**(7), (1998), 863-888.

Brace, W. F., And. Bombolakis, E. G..: A Note On Brittle Crack Growth in Compression, *Journal of Geophysical Research*, **68**(12): (1963), 3709-3713.

Cannon, N. P., et al.: Wing Cracks and Brittle Compressive Fracture, *Acta Metallurgica Et Materialia*, **38**(10), (1990), 1955-1962.

Chen, G., et al.: Fracture Propagation and Coalescence in Marble Plates with Pre-Cut Notches Under Compression, *Proceedings*, Symposium on Fractured and Jointed Rock Mass, Lake Tahoe, CA (1992).

Cheng, Q., and Ghassemi, A.: Numerical Modeling of Newberry EGS Stimulation, *Proceedings*, 50th US Rock Mechanics/Geomechanics Symposium, American Rock Mechanics Association, Houston, TX (2016).

Cornet, F., et al.: How Close to Failure Is a Granite Rock Mass at A 5 Km Depth? *International Journal of Rock Mechanics and Mining Sciences*, **44**(1), (2007), 47-66.

Crawford, B., et al.: Incorporating Universal Scaling of Fracture Stiffness and Surface Roughness Effects for Improved Productivity Prediction in Naturally Fractured Reservoirs, *Proceedings*, 50th US Rock Mechanics/Geomechanics Symposium, American Rock Mechanics Association, Houston, TX (2016).

Durham, W., and Bonner, B.: Self-Propping and Fluid Flow in Slightly Offset Joints at High Effective Pressures, *Journal of Geophysical Research: Solid Earth*, **99**(B5), (1994), 9391-9399.

Esaki, T., et al.: Shear-Flow Coupling Test on Rock Joints, *Proceedings*, 7th ISRM Congress, International Society for Rock Mechanics, (1991).

Evans, K. F.: Permeability Creation and Damage Due to Massive Fluid Injections into Granite at 3.5 Km at Soultz: 2. Critical Stress and Fracture Strength, *Journal of Geophysical Research: Solid Earth*, **110**(B4), (2005).

Evans, K. F., et al.: Permeability Creation and Damage Due to Massive Fluid Injections into Granite at 3.5 Km at Soultz: 1. Borehole Observations, *Journal of Geophysical Research: Solid Earth*, **110**(B4), (2005).

Goncalves Da Silva, B., et al.: Development of A Test Setup Capable of Producing Hydraulic Fracturing in The Laboratory with Image and Acoustic Emission Monitoring, *Proceedings*, 49th U.S. Rock Mechanics/Geomechanics Symposium, American Rock Mechanics Association, San Francisco, CA (2015).

Hofmann, H., et al.: Transmissivity of Aligned and Displaced Tensile Fractures in Granitic Rocks During Cyclic Loading, *International Journal of Rock Mechanics and Mining Sciences*, **87**, (2016), 69-84.

Huang, D., et al.: Investigation On Mechanical Behaviors of Sandstone with Two Preexisting Flaws Under Triaxial Compression, *Rock Mechanics and Rock Engineering*, **49**(2): (2016), 375-399.

Huang, K., et al.: Modeling Three-Dimensional Hydraulic Fracture Propagation Using Virtual Multidimensional Internal Bonds, *International Journal for Numerical and Analytical Methods in Geomechanics*, **37**(13), (2013), 2021-2038.

Jung, R.: EGS — Goodbye or Back to The Future 95, *Effective and Sustainable Hydraulic Fracturing*, InTech: Ch. 05, (2013).

Kamali, A., and Ghassemi, A.: Analysis of Natural Fracture Shear Slip and Propagation in Response to Injection, *Proceedings*, Stanford Geothermal Workshop, Stanford, CA (2016).

Lee, H., and Jeon, S.: An Experimental and Numerical Study of Fracture Coalescence in Pre-Cracked Specimens Under Uniaxial Compression, *International Journal of Solids and Structures*, **48**(6), (2011) 979-999.

Li, B., et al.: Experimental Study of the Hydro-Mechanical Behavior of Rock Joints Using a Parallel-Plate Model Containing Contact Areas and Artificial Fractures, *International Journal of Rock Mechanics and Mining Sciences*, **45**(3), (2008), 362-375.

Liu, X. W., et al.: Fracture Propagation Characteristic and Micromechanism of Rock-Like Specimens Under Uniaxial and Biaxial Compression, *Shock and Vibration*, (2016).

McClure, M., and Horne, R.: Conditions Required for Shear Stimulation in EGS, *Proceedings*, 2013 European Geothermal Congress, Pisa, Italy (2013).

Miller, J. T., and Einstein, H. H.: Crack Coalescence Tests On Granite, *Proceedings*, 42nd U.S. Rock Mechanics Symposium (USRMS). American Rock Mechanics Association, San Francisco, CA (2008).

Min, K. S., et al.: Numerical Analysis of Multiple Fracture Propagation in Heterogeneous Rock, *Proceedings*, 44th U.S. Rock Mechanics Symposium and 5th U.S.-Canada Rock Mechanics Symposium, American Rock Mechanics Association, Salt Lake City, Utah (2010).

Modiriasari, A., et al.: Monitoring Rock Damage Caused by Cyclic Loading Using Seismic Wave Transmission and Reflection, *Proceedings*, 50th U.S. Rock Mechanics/Geomechanics Symposium, American Rock Mechanics Association, Houston, TX (2016).

Morgan, S., et al.: Effect of Injection Rate On Hydraulic Fracturing of Opalinus Clay Shale, *Proceedings*, 51st US Rock Mechanics/Geomechanics Symposium, American Rock Mechanics Association, San Francisco, CA (2017).

Mughieda, O., and Karasneh, I.: Coalescence of Offset Rock Joints Under Biaxial Loading, *Geotechnical & Geological Engineering*, **24**(4): (2006), 985.

Nemat-Nasser, S., and Horii, H.: Compression-Induced Nonplanar Crack Extension with Application to Splitting, Exfoliation, And Rockburst, *Journal of Geophysical Research: Solid Earth*, **87**(B8), (1982), 6805-6821.

Nemoto, K., et al.: Mechanical and Hydraulic Coupling of Injection-Induced Slip Along Pre-Existing Fractures, *Geothermics*, **37**(2), (2008), 157-172.

Nygren, A., and Ghassemi, A.: Influence of Cold Water Injection On Critically Stressed Fractures in Coso Geothermal Field, CA, *Proceedings*, 40th US Symposium On Rock Mechanics (USRMS), American Rock Mechanics Association, Alaska (2005).

Park, H., et al.: Development of Coupled Shear-Flow-Visualization Apparatus and Data Analysis, *International Journal of Rock Mechanics and Mining Sciences*, **63**, (2013), 72-81.

Petit, J. P., and Barquins, M.: Can Natural Faults Propagate Under Mode II Conditions? *Tectonics*, **7**(6), (1988), 1243-1256.

Pine, R. J., and Batchelor, A. S.: Downward Migration of Shearing in Jointed Rock During Hydraulic Injections, *International Journal of Rock Mechanics and Mining Sciences & Geomechanics Abstracts*, **21**(5): (1984), 249-263.

Rahman, M., et al.: A Shear-Dilation-Based Model for Evaluation of Hydraulically Stimulated Naturally Fractured Reservoirs, *International Journal for Numerical and Analytical Methods in Geomechanics*, **26**(5): (2002), 469-497.

Saimoto, A., and Nisitani, H.: Crack Propagation Criterion and Simulation Under Biaxial Loading, *WIT Transactions On Engineering Sciences* 37, (2002).

Willis-Richards, J., et al.: Progress Toward a Stochastic Rock Mechanics Model of Engineered Geothermal Systems, *Journal of Geophysical Research: Solid Earth*, **101**(B8), (1996), 17481-17496.

Wong, L. N. Y., and Einstein, H. H. Systematic Evaluation of Cracking Behavior in Specimens Containing Single Flaws Under Uniaxial Compression, *International Journal of Rock Mechanics and Mining Sciences*, **46**(2): (2009), 239-249.

Yang, S., et al.: Experimental Investigation on Strength and Failure Behavior of Pre-Cracked Marble Under Conventional Triaxial Compression, *International Journal of Solids and Structures*, **45**(17): (2008), 4796-4819.

Ye, Z., et al.: Experimental Investigation of Injection-Driven Shear Slip and Permeability Evolution in Granite for EGS Stimulation, *Proceedings*, 42nd Workshop On Geothermal Reservoir Engineering, Stanford, CA (2017).

Ye, Z., et al.: Injection-Driven Shear Slip and The Coupled Permeability Evolution of Granite Fractures for EGS Stimulation, *Proceedings*, 51st US Rock Mechanics / Geomechanics Symposium, American Rock Mechanics Association, San Francisco, CA (2017).

Ye, Z., et al.: Laboratory Investigation of Permeability Evolution in Shear Stimulation of Granite Fractures for EGS, *Proceedings*, 41st GRC Annual Meeting, Salt Lake City, Utah (2017).

Ye, Z., et al.: Laboratory Investigation of Fluid Flow and Permeability Evolution Through Shale Fractures, *Proceedings*, Unconventional Resources Technology Conference (URTeC), Austin, TX (2017).

Yeo, I. W., et al.: Effect of Shear Displacement on the Aperture and Permeability of a Rock Fracture, *International Journal of Rock Mechanics and Mining Sciences*, **35**(8), (1998), 1051-1070.

Yin, P., et al.: Crack Growth and Coalescence Mechanism in Granite Material Containing Two Surface Flaws Under Uniaxial Compression, *Proceedings*, 44th U.S. Rock Mechanics Symposium and 5th U.S.-Canada Rock Mechanics Symposium, American Rock Mechanics Association, Salt Lake City, Utah (2010).

Zhang, Z., et al.: Micro-and Macro-Behaviour of Fluid Flow Through Rock Fractures: An Experimental Study, *Hydrogeology Journal*, **21**(8), (2013), 1717-1729.